DEU FMD 28(84) (2026) 470-479

Dokuz Eylül Üniversitesi Mühendislik Fakültesi Fen ve Mühendislik Dergisi
Dokuz Eylul University Faculty of Engineering Journal of Science and Engineering
Elektronik/Online ISSN: 2547-958X

RESEARCH ARTICLE / ARAŞTIRMA MAKALESI

Effect of Hole-Making Strategy on the Mechanical Performance of 3D FDM-Printed Polymers

Delik Açma Stratejisinin 3B FDM Baskılı Polimerlerin Mekanik Performansına Etkisi

Emre Akın [1*], Murat Şen [2]

[1] Marmara Üniversitesi Teknoloji Fakültesi Metalurji ve Malzeme Mühendisliği Bölümü, İstanbul, TÜRKİYE
[2] Marmara Üniversitesi Teknoloji Fakültesi Makine Mühendisliği Bölümü, İstanbul, TÜRKİYE

Corresponding Author / Sorumlu Yazar *: emre.akin@marmara.edu.tr

Abstract

In this research, the effect of hole-making technique on the mechanical properties of FDM-printed polymers is examined. Four common materials (ASA, PETG, Tough PLA, and Hyper PLA) were tested in three types of specimens: no-hole (NH), in-situ hole-printed (PH), and micro-drilled hole (DH). Tensile testing, SEM evaluation, Vicat softening temperature, and melt flow index (MFI) tests were performed. PH specimens demonstrated a systematic decrease in tensile strength and modulus for all materials. DH specimens presented enhanced stiffness for all materials and improved tensile strength for PETG (16.3%) and Tough PLA (7.6%), but strength degradation for ASA and Hyper PLA compared to NH specimens. Surface roughness measurements demonstrated significantly lower Ra values for DH samples compared to PH samples, validating better hole-edge surface quality after drilling. SEM analysis confirmed ring-shaped failure areas around PH and more compact and smooth areas around DH. The mechanical properties were explained in the context of the thermal and rheological properties of each polymer material. The findings of this study clearly show that hole-making techniques have a significant impact on the structural properties of FDM-printed parts.

Keywords: *Fused Deposition Modeling (FDM), Hole-Making Strategy, Mechanical Properties, Micro-Drilling*

Öz

Bu çalışmada, FDM yöntemiyle üretilmiş polimerlerin mekanik özellikleri üzerindeki delik açma tekniğinin etkisi incelenmiştir. Dört yaygın malzeme (ASA, PETG, Tough PLA ve Hyper PLA), üç farklı numune tipinde test edilmiştir: deliksiz (NH), üretim sırasında basılmış delikli (PH) ve mikro-delme ile oluşturulmuş delikli (DH). Çekme testleri, SEM incelemeleri, Vicat yumuşama sıcaklığı ve eriyik akış indeksi (MFI) testleri gerçekleştirilmiştir. PH numuneleri, tüm malzemelerde çekme dayanımı ve elastik modülde sistematik bir azalma göstermiştir. DH numuneleri ise tüm malzemelerde artan rijitlik sergilemiş; PETG (%16,2) ve Tough PLA (%7,5) için çekme dayanımında iyileşme sağlarken, ASA ve Hyper PLA'da NH numunelere kıyasla dayanım düşüşü gözlenmiştir. Yüzey pürüzlülüğü ölçümleri, DH numunelerinde PH numunelere kıyasla belirgin derecede daha düşük Ra değerleri olduğunu göstermiş ve delme işlemi sonrasında daha iyi delik-kenarı yüzey kalitesini doğrulamıştır. SEM analizleri, PH numunelerinde halka şeklinde hasar bölgeleri ve DH numunelerinde daha kompakt ve düzgün morfolojik bölgeler ortaya koymuştur. Mekanik özellikler, her bir polimerin termal ve reolojik özellikleri bağlamında açıklanmıştır. Bu çalışmanın bulguları, delik açma tekniklerinin FDM ile üretilmiş parçaların yapısal özellikleri üzerinde önemli bir etkiye sahip olduğunu açıkça göstermektedir.

Anahtar Kelimeler: *Eriyik Yığma Modelleme (FDM), Delik Oluşturma Stratejisi, Mekanik Özellikler, Mikro Delme*

1. Introduction

Additive Manufacturing (AM) technologies, particularly Fusion Deposition Modeling (FDM), have gained significant attention in various industries due to their ability to create complex geometries, reduce material waste, and offer design flexibility. FDM is widely used because of its low cost, material diversity, and capacity for producing both functional and structural components [1]. The advantageous properties of FDM, including its compatibility with materials such as PLA, ABS, PETG, and composite filaments reinforced with carbon or glass fiber, enable its application across various sectors, including the automotive, aerospace, and medical industries [2,3].

As FDM technology advances from rapid prototyping to the fabrication of functional end-use parts, the addition of geometric details like holes to the printed parts has become a subject of growing interest. In particular, micro-holes have become essential in high-precision engineering applications. Industries such as automotive, aerospace and electronics utilize micro-holes in components including injectors, turbines, watch mechanisms, and printed circuit boards. These features are critical for achieving tight dimensional tolerances, precise geometries, and high surface quality, all of which are crucial for the integration of complex and compact systems [4,5]. In addition to their functional use, holes are also used for the purpose of reducing weight, enhancing heat transfer, and optimizing structures. However, the mechanical performance of FDM-manufactured parts is significantly affected by the presence, size, and placement of holes [6]. Holes can be considered as stress concentrators that lead to a reduction in the structural integrity of a part; on the other hand, they can also be used to enhance the distribution of loads and minimize the use of material without affecting the mechanical integrity of the part. Additionally, previous studies have demonstrated that interlayer voids and structural defects adversely affect the mechanical performance of 3D-printed components, resulting in a reduction in overall strength [8,9].

DOI: https://doi.org/10.21205/deufmd.2026288414

Geliş Tarihi / Received: 15.10.2025
Kabul Tarihi / Accepted: 12.03.2026

Hence, the addition of holes to such structures is also expected to affect stress distribution.

In FDM fabrication, holes can be produced either directly during fabrication as built-in geometries or after fabrication through post-processing techniques such as mechanical drilling. Each approach offers distinct advantages and limitations, with the choice depending largely on the specific application, material properties, and desired precision.

Integrating hole-making directly into the printing process is one of the main advantages of additive manufacturing, enabling the creation of complex and customized shapes that are difficult or impossible to achieve with traditional manufacturing techniques. This method eliminates the need for secondary machining processes, resulting in significant reductions in material waste and overall production time. However, the production of high-dimensional accuracy for small or complex holes is difficult because the low resolution of the nozzle and stepper motor system commonly results in surface roughness and dimensional errors, which can significantly reduce the local mechanical properties [10].

Hernandez et al. [11] demonstrated experimentally that factors such as shell thickness, part size, and printing speed are correlated with dimensional errors. Specifically, they observed that smaller hole sizes are associated with greater mean dimensional deviations. Knoop et al. [12] reported that holes with diameters smaller than 18 mm tend to be undersized when 3D-printed. Moreover, material properties also play an important role in hole accuracy during fabrication. Thermoplastics may exhibit warping or shrinkage during the cooling process, further complicating efforts to achieve accurate and consistent hole dimensions [13]. In contrast, holes produced through mechanical drilling typically exhibit superior dimensional accuracy and smoother surface finishes, potentially enhancing local structural integrity [14,15]. Schmeier et al. [6] investigated hole-making methods in 3D-printed PLA specimens and compared printed holes with drilled holes. The results showed that printed holes have rougher surfaces, leading to higher stress concentrations, whereas drilled holes produce smoother edges and more consistent geometries. Rao et al. [16] compared the tensile strength of FDM-printed composites containing pre-defined holes with conventionally drilled composites and reported superior tensile strength for the drilled specimens. Nevertheless, the drilling operation may cause thermal and mechanical stresses depending on the drilling tool geometry, feed rate, and thermal properties of the printed polymer. These factors may alter the microstructure around the drilled region and influence the overall mechanical behavior of the part. Moreover, a study on drilling composites with varying hole diameters indicated that measurement error increases with increasing hole diameter [17], which should be considered when applying conventional drilling to FDM parts.

In addition to the mechanical aspect, the two hole creation techniques are also different in processing time and cost effectiveness. Post-processing operations such as drilling introduce additional time and cost to the manufacturing workflow due to extra steps and specialized equipment requirements [18]. Both techniques are widely used in part manufacturing based on FDM technology. Nevertheless, the effect of the hole creation technique on the mechanical properties is still a major concern, especially for parts loaded in tension or cyclic loading. Understanding the implications of each approach is crucial for optimizing design decisions in functional 3D-printed applications. Despite the common application of holes in joined and functional components, very few studies have been conducted to systematically compare these two hole-making methods in commonly used FDM filaments. The literature gap emphasizes the importance of this study, which intends to compare the mechanical properties of components made by different hole-making methods and widely used FDM materials.

In this study, tensile specimens were prepared from four different materials: ASA, PETG, Tough PLA, and Hyper PLA, and divided into three specimen categories. In the first class, micron-scale holes were introduced at the center of the tensile bars by micro-drilling (DH samples). In the second class, the same holes were produced in situ during fabrication on the FDM printer (PH samples). The third class consisted of specimens without holes. All three classes were characterized by tensile testing, and their ultimate tensile strength, Young's modulus, and elongation at break were compared. In addition, scanning electron microscopy (SEM) was used to examine fracture surfaces and identify printing defects, providing complementary insight into the mechanical results. The thermal and rheological properties of the materials were also investigated by Vicat softening temperature and melt flow index (MFI) tests, and the results were interpreted in relation to commercial filament materials.

2. Materials and Methods

In this study, ASA (Acrylonitrile Styrene Acrylate), Tough PLA (Polylactic Acid), Hyper PLA and PETG (Polyethylene Terephthalate Glycol) were employed based on their material properties and suitability for specific applications. These filaments are widely used in 3D printing due to their reliable performance across a range of applications, with each offering distinct advantages [19,20]. ASA was selected for its superior UV resistance and durability under environmental conditions, while PLA was chosen for its environmentally friendly, biodegradable nature and its ability to print at low temperatures, making it ideal for prototyping. PETG, known for its durability, flexibility, and chemical resistance, was also considered for applications requiring strength and resilience. All filaments were provided by the manufacturer, Porima 3D and their properties are detailed in Table 1 [21].

Table 1. The properties of ASA, Tough PLA, Hyper PLA and PETG commercial filaments [21].

Material properties		ASA	Tough PLA	Hyper PLA	PETG
Physical properties	Density (g/cm^3)	1.06	1.22	1.23	1.28
	Melted flow index (g/10min)	22	17.3	17.3	20
Mechanical properties	Tensile Strength (MPa)	48	50	56	53
	Elastic Modulus (GPa)	2.1	2.4	2.85	3.0
	Elongation at Break (%)	12	50	7	30
	Impact strenght (kJ/m^2)	17	36	14.2	14.2
Thermal properties	Heat deflection temperature (°C)	95	58	55	80
	Transition temperature (°C)	100-105	55-65	55-60	80-85

The 3D models were designed using SolidWorks and converted into STL format to ensure compatibility with the 3D printing process. Experimental test specimens were fabricated using an

Elegoo Neptune 4 Pro 3D printer with 100% infill density, a layer height of 0.05 mm and a nozzle diameter of 0.4 mm. Printer-specific settings defined in the Orca Slicer software were applied during manufacturing. For filament settings, the generic presets provided by the software for each material type were used. Nozzle temperatures were set based on the average of the minimum and maximum extrusion temperatures recommended by the manufacturer, while the bed temperature was set to the maximum advised value. All specimens were printed with linear infill patterns on a heated bed without any support structures. Table 2 summarizes the printing process parameters used in this study. Following the printing process, support structures were removed and surface finishing was applied. The parts were then inspected for dimensional accuracy and surface quality.

Table 2. The printing process parameters for each filament type [21].

Material	Nozzle Temperature (°C)	Bed Temperature (°C)	Print Speed (mm/s)	Layer thickness (mm)	Cooling Fan Settings
ASA	260	100	200	0.05	Disabled
Tough PLA	235	60	200	0.05	100% after first layer
Hyper PLA	235	60	200	0.05	100% after first layer
PETG	240	80	200	0.05	20% after first layer

Figure 1 provides a graphical representation of the methodology. For each material type, three types of specimens were prepared as shown in Figure 1b: control specimens without holes (No hole - NH), specimens with holes integrated during printing (Printed hole - PH) and specimens with holes drilled post-production (Drilled hole - DH). The holes are positioned perpendicular to the loading axis and symmetrically around the geometric center of the specimens. Figure 1c illustrates that the specimen geometry was designed in accordance with the ASTM D638 Type IV standard for tensile testing [22]. The characterization processes performed on the specimens are given in Figures 1d and 1e. Tensile tests were conducted using a Zwick Z010 testing machine at a crosshead speed of 5 mm/min under ambient temperature conditions. The analysis focused on ultimate tensile strength, Young's modulus, elongation at break and energy absorption, calculated from the area under the stress–strain curve. For each type of sample (code), five specimens were prepared, and the values reported are the average of these five specimens. Following tensile testing, the fracture surface morphologies were investigated using a Carl Zeiss Ultra Plus scanning electron microscope (SEM) at an acceleration voltage of 20 kV. Before the SEM analysis, the specimens were coated with a 2-4 nm layer of Au/Pd using a Quorum Q150R device in an ion beam sputtering system.

For the DH specimens, the micro-drilling process was performed using a Johnford VMC-550 CNC machine. The experimental setup for this process is illustrated in Figure 2. The test parts were fixed to the fixture by applying adhesive to both corners. The gap provided by the fixture effectively prevented tool breakage during the drilling process. Drilling was carried out under dry conditions using a two-flute tungsten carbide micro drill. The tool had a nominal diameter of 1000 µm, a point angle of 118° and a helix angle of 30°. To eliminate the effect of tool wear as a variable, a new drill bit was used for each operation. Process parameters of the drilling process are given in Table 3. Due to the characteristics of the materials, different parameters were used in the drilling process. Considering the high elastic modulus of Tough PLA and Hyper PLA, which typically exerts greater mechanical stresses on cutting tools during machining and increases the risk of tool failure, the feed rate was decreased to prevent tool breakage.

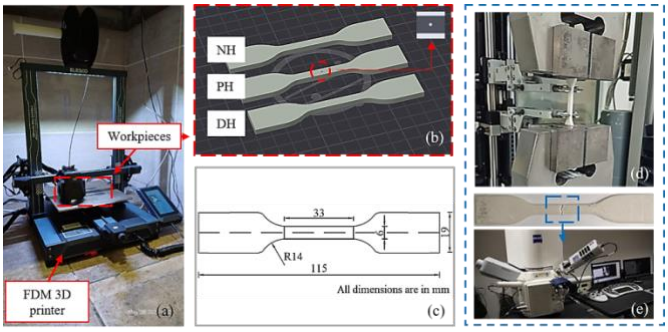

Figure 1. (a) Experimental setup (b) types of specimens (c) dimensions produced according to ASTM D638 Type IV standard (d) tensile test (e) SEM analysis.

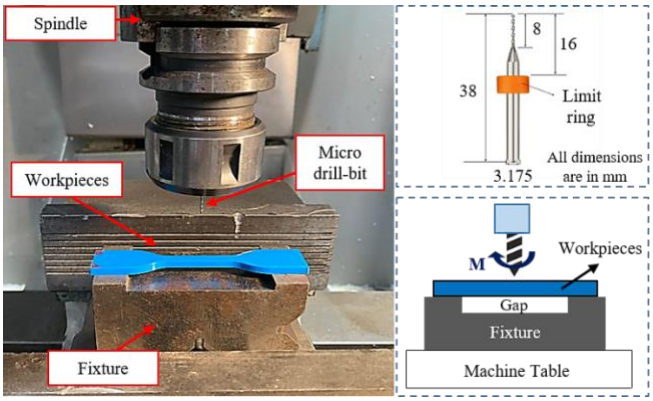

Figure 2. Schematic diagram of the drilling process.

Table 3. The drilling process parameters for each filament type.

Material	ASA	Tough PLA	Hyper PLA	PETG
Spindle speed, V (rpm)	750	1000	1000	750
Feed rate, f (mm/min)	2.0	1.0	1.0	2.0

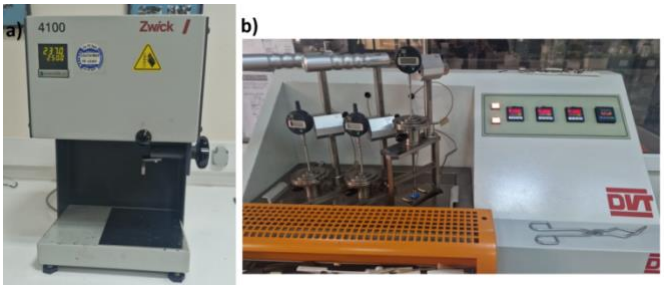

Figure 3. Photographic views of the experimental setups: (a) melt flow index (MFI) testing device and (b) Vicat softening temperature testing device.

The melt flow index (MFI) tests were conducted to evaluate the flow behavior of the four 3D-printed thermoplastic materials (ASA, Tough PLA, Hyper PLA, and PETG). For each material, three replicate measurements were performed. The printed specimens were first cut into small particulate pieces to ensure uniform melting, and approximately 10 g of these particles were loaded into the MFI apparatus. Before each test, the device was preheated to the corresponding melting temperature of the respective material to ensure thermal equilibrium and consistent flow behavior. Once the target temperature was reached, the material was allowed to melt completely, and the molten polymer was extruded through a calibrated orifice under a constant load. The mass of the extrudate obtained within one minute (g/min) was recorded and subsequently converted to the standard unit of g/10 min. Testing conditions were selected in accordance with the recommendations of the ASTM D1238 standard and optimized for each polymer type. The PLA-based materials (Tough PLA and Hyper PLA) were tested at 190 °C under a load of 2.16 kg, ASA at 220 °C under a load of 5 kg, and PETG at 250 °C under a load of 2.16 kg. These parameters were chosen to reflect the typical extrusion and softening behavior of each polymer. The experimental setups for both tests are shown in Figure 3.

The Vicat softening temperature tests were performed to assess the thermal resistance of the printed materials to surface deformation under load. Two specimens of each material, with nominal dimensions of 30 × 30 × 4 mm, were prepared. The specimens were immersed in silicone oil to ensure uniform heat transfer, and the Vicat indenter (1 mm^2 tip area) was positioned vertically on the specimen surface under a standard load of 10 N. The oil bath temperature was increased at a controlled rate of 50 °C h^{-1} until the indenter penetration reached 1 mm, and the corresponding temperature was recorded as the Vicat softening temperature. The procedure followed the general guidelines of ASTM D1525.

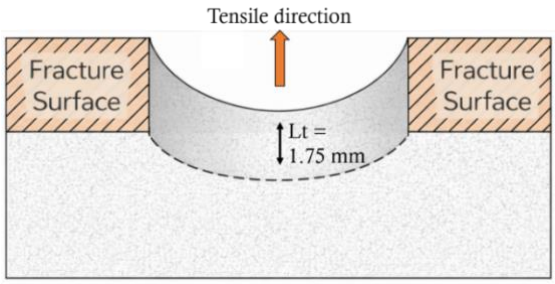

Figure 4. Schematic of internal hole surface used for roughness measurement.

Surface roughness measurements were conducted using a contact surface profilometer (Mahr Perthometer M2) to quantitatively compare the surface quality of printed-hole (PH) and drilled-hole (DH) specimens and to examine the influence of hole-edge surface quality on tensile strength and elongation behavior, as schematically illustrated in Figure 4. Tensile tests were first performed, after which the internal hole surfaces became accessible as semi-cylindrical regions. Surface roughness was then measured directly on these internal hole surfaces, excluding the fracture surface and plastically deformed regions, in order to characterize the original hole-edge surface responsible for crack initiation. Measurements were taken along the hole axis with a cut-off length (Lc) of 0.25 mm and an evaluation length (Lt) of 1.75 mm, which corresponds to the minimum evaluation length permitted by the device and satisfies the ISO 4288 requirement (Lt ≥ 5×Lc). For each specimen, measurements were repeated three times at different axial positions, and the average Ra value was reported in Table 4 .

3. Results and Discussion

This discussion focuses on the mechanical and morphological behavior of ASA, PETG, Tough PLA, and Hyper PLA specimens with no holes (NH), printed holes (PH), and micro-drilled holes (DH). The effect of hole-making methods on tensile strength, stiffness, ductility, and failure modes is presented in the context of thermal and rheological properties of the materials. Moreover, the surface roughness of the hole-edge areas at the fracture sections was investigated to better understand the effect of local surface quality on mechanical properties. As the effect of hole-making methods on the mechanical performance of FDM parts has not been adequately explored in the existing literature, this discussion is intended to relate the findings to the quality of interlayer bonding, stress concentration effects, material flow properties, and hole-edge surface quality. Table 4 summarizes the mechanical results, and Figure 5 shows the stress-strain curves.

3.1. Ultimate Tensile Strength

Table 4 summarizes the ultimate tensile strength (UTS) of the samples. For no-hole specimens, UTS values were 48.3 MPa for ASA, 38.1 MPa for PETG, 46.1 MPa for Tough PLA, and 47.5 MPa for Hyper PLA. Drilled-hole specimens showed a mixed response: Tough PLA-DH reached 49.6 MPa, which represents an increase of about 7.6 % compared with its no-hole counterpart, while PETG-DH rose to 44.3 MPa, corresponding to an improvement of approximately 16.3 %. Conversely, ASA-DH decreased to 42.8 MPa, indicating a reduction of about 11.4 %, and Hyper PLA-DH dropped to 40.9 MPa, a decline of roughly 13.9 % relative to their no-hole specimens, although both still exhibited higher strength than their printed-hole counterparts. Printed-hole specimens consistently showed the lowest UTS across all materials: 39.5 MPa for ASA (18 % lower), 22.6 MPa for PETG (41 % lower), 28.9 MPa for Tough PLA (37 % lower), and 34.3 MPa for Hyper PLA (28 % lower) than their no-hole references. These findings suggest that although micro-drilling can preserve or even improve tensile strength depending on the type of polymer, in-situ hole printing tends to reduce the load-bearing area and the bonding between layers [6,10,16].

3.2. Young's Modulus

Young's modulus values for no-hole specimens were 1953.9 MPa for ASA, 1951.6 MPa for PETG, 2794.3 MPa for Tough PLA, and 2853.8 MPa for Hyper PLA. Drilled-hole specimens exhibited a clear stiffness gain: ASA-DH rose to 2259.6 MPa, representing an increase of about 15.6 %; PETG-DH climbed to 2059.1 MPa, an improvement of roughly 5.5 %; Tough PLA-DH reached 3094.1 MPa, corresponding to a 10.7 % increase; and Hyper PLA-DH achieved 2881.0 MPa, a slight rise of around 1 %. Printed-hole specimens, however, showed minor reductions: ASA-PH recorded 2103.3 MPa (approximately 7.6 % higher than its no-hole value but still below DH), PETG-PH dropped to 1848.5 MPa, about 5.3 % lower; Tough PLA-PH fell to 2689.2 MPa, 3.8 % lower; and Hyper PLA-PH declined to 2778.0 MPa, 2.7 % lower compared with their no-hole references. In general, micro-drilling helped improve stiffness compared to no-hole specimens, while in-situ hole printing resulted in low but systematic reductions [14,15].

3.3. Elongation at Break

Elongation at break values for the no-hole specimens were 9.4 % for ASA, 2.6 % for PETG, 2.0 % for Tough PLA and 4.3 % for Hyper PLA. Micro-drilling tended to reduce ductility: ASA-DH dropped to 2.3 %, representing a decrease of about 76 % relative to the no-hole specimen; Hyper PLA-DH fell to 1.8 % (a decrease of roughly 58 %); Tough PLA-DH fell slightly to 1.8 % (about 10 %

lower), while PETG-DH remained essentially unchanged at 2.6 %. Printed-hole specimens exhibited the lowest elongation at break across all materials. ASA-PH decreased to 2.0 %, which is roughly 79 % lower than the no-hole specimen. PETG-PH decreased to 1.3 %, about 50 % lower. Tough PLA-PH dropped to 1.1 %, around 45 % lower, and Hyper PLA-PH to 1.26 %, about 71 % lower than its no-hole counterpart. These data indicate that although drilled holes introduce stress concentrators, the loss of ductility is moderate for most materials, whereas producing the hole in situ during printing leads to a pronounced reduction in elongation at break, especially for ASA and Hyper PLA. This reduction in strain-to-failure, combined with the already lower tensile strength of PH specimens, yields a substantial decrease in overall toughness (area under the stress–strain curve) relative to both no-hole and drilled-hole specimens [8-10].

Table 4. Mechanical properties and hole-edge roughness values of the samples.

Samples	Ultimate Tensile Strength (MPa)	Young's Modulus (MPa)	Elongation at Break (%)	Ra (µm)
ASA	48.3±1.76	1953.9±46.7	9.4±0.74	-
ASA-DH	42.8±1.56	2259.6±0.54	2.3±0.18	3.1
ASA-PH	39.5±1.44	2103.3±50.2	2.0±0.16	9.1
Tough PLA	46.1±1.68	2794.3±66.7	2.0±0.16	-
Tough PLA-DH	49.6±1.81	3094.1±73.9	1.8±0.14	2.6
Tough PLA-PH	28.9±1.05	2689.2±65.2	1.1±0.09	12.3
Hyper PLA	47.5±1.73	2853.8±68.1	4.3±0.34	-
Hyper PLA-DH	40.9±1.49	2881.0±68.8	1.8±0.14	2.8
Hyper PLA-PH	34.3±1.25	2778.0±66.3	1.26±0.10	11.4
PETG	38.1±1.39	1951.6±46.6	2.6±0.21	-
PETG-DH	44.3±1.62	2059.1±49.2	2.6±0.21	2.2
PETG-PH	22.6±0.82	1848.5±44.1	1.3±0.10	13.7

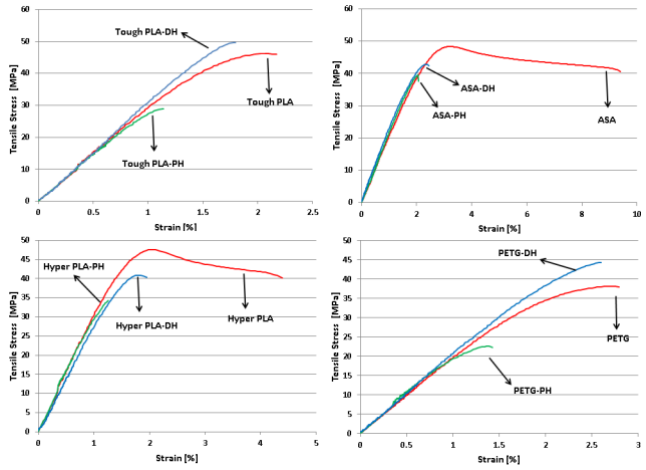

Figure 5. Tensile stress-strain curves of the samples.

When the failure process of the specimens is considered from the tensile stress-strain curves, two distinct material behaviors can be identified. ASA and Hyper PLA have similar failure properties. After the ultimate tensile strength, these materials have a gradual decrease in stress with a continuous increase in strain, showing the onset of necking before the final break. This post-peak deformation is a sign of localized plastic deformation and is most evident in the no-hole specimens, where the failure is postponed after the UTS.

Tough PLA and PETG have a similar but different failure process. For these materials, failure happens shortly after the maximum stress is attained with very little deformation after the UTS. The stress values decrease more rapidly after the peak, showing more brittle failure than ASA and Hyper PLA. To be specific, the elongation at UTS for ASA is about 3%, and Hyper PLA attains the UTS at about 1.95% strain. For these two materials, necking is more prominent, as indicated by the fairly large value of the difference between elongation at UTS and elongation at break. By contrast, Tough PLA has an elongation at UTS of about 2%, while PETG has an elongation at UTS of about 2.75%. However, for Tough PLA and PETG, the elongation at break is practically the same as the elongation at UTS, which means that crack initiation and final fracture occur almost simultaneously with little post-peak deformation.

The effect of hole-making methods also impacts the failure process. Printed-hole (PH) and drilled-hole (DH) specimens have less strain capacity than no-hole specimens for all materials. For most PH and DH specimens, the strain at UTS is practically the same as the strain at break, which means that crack initiation and final fracture occur within a very short strain range. This means that the first load drop due to crack initiation occurs at a strain level close to the UTS strain, especially for specimens with holes.

3.4 Morphological Observations

The morphologies and mechanical properties of the specimens are summarized in Figure 6, 7, 8, 9, 10, and 11. Figure 6 shows the macroscopic morphologies of the fractured specimens after tensile testing. Figure 7 and 8 describe the trends of the mechanical properties derived from the tensile testing results. Figure 9, 10, and 11 describe the morphological details, including the interlayer structure and the surface conditions around the drilled and printed holes.

Figure 7 reveals distinct fracture characteristics among the three specimen types, namely no-hole (NH), micro-drilled (DH), and printed-hole (PH), for all four materials (ASA, Hyper PLA, Tough PLA, and PET-G).

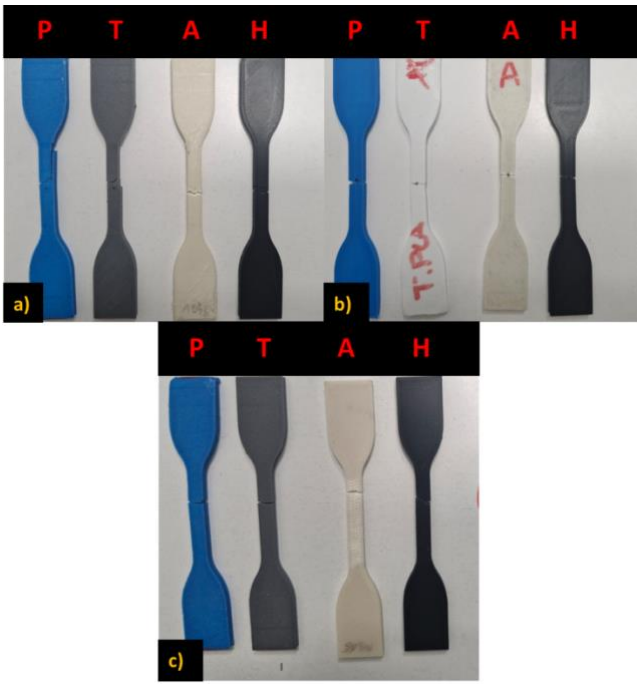

Figure 6. Fracture appearances of (a) printed-hole (PH), (b) drilled-hole (DH), and (c) hole-free samples (NH) after tensile testing (P: PETG, T: Tough PLA, A: ASA, H: Hyper PLA).

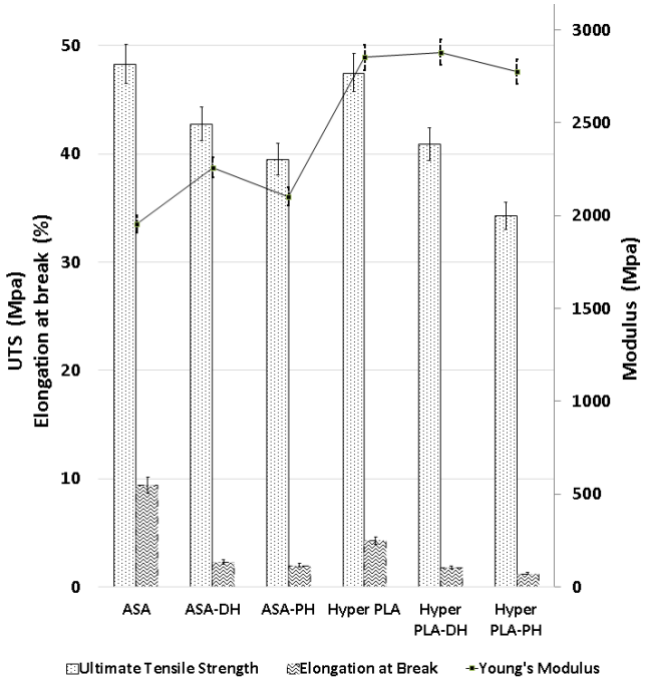

Figure 7. Trends in mechanical properties derived from tensile test results of ASA and Hyper PLA samples.

Notably, all micro-drilled specimens showed crack initiation at the micro-drilled holes, and this indicates that the stress concentration and defects at the drilled area were the major crack origins. This is an indication that the drilling process created micro-level stress risers that contributed to the formation of early cracks [7,16,17].

By contrast, the PH specimens had a fracture pattern that was quite different from the other specimens, in that instead of breaking through the hole, the fracture propagated around the hole in a ring-like fashion that was slightly offset from the edge of the hole [10–12]. As illustrated in Figure 6, this behavior aligns with Rankouhi et al. [10]'s findings, who reported that "the limited resolution of the nozzle and stepper motor system can lead to surface roughness, dimensional inaccuracies, and significantly degrade local mechanical performance." In the present work, such local irregularities appear to generate subtle stress accumulations around the hole boundary, resulting in the observed ring-like fracture morphology.

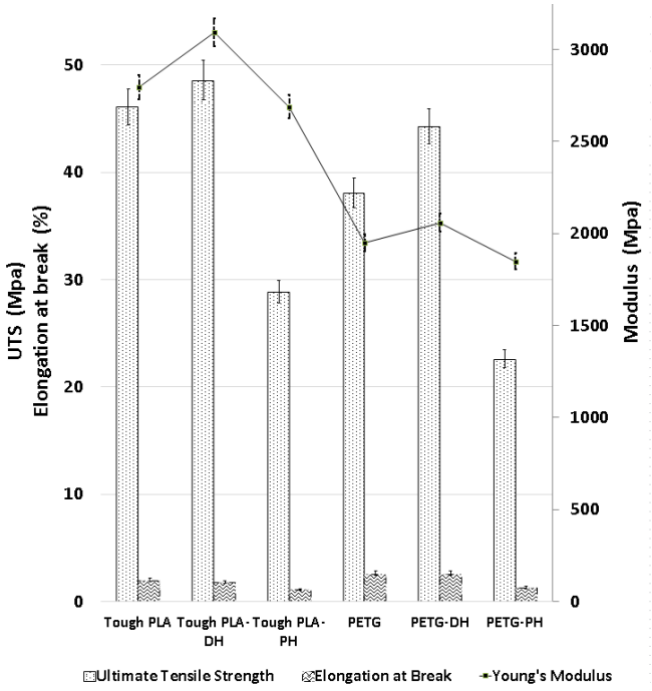

Figure 8. Trends in mechanical properties derived from tensile test results of Tough PLA and PETG samples.

Figure 9, 10, and 11 further show SEM micrographs of tensile-fractured surfaces for the three types of specimens. From the no-hole specimens shown in Figure 6, the layer boundaries are clearly defined, which is typical of FDM-printed specimens [8–10]. Consistent with the mechanical test results, ASA exhibited the most ductile fracture morphology, with elongated fibrillar regions indicative of plastic deformation. Both ASA and Tough PLA displayed relatively thick deposited layers likely due to partial over-extrusion during printing, whereas Hyper PLA and PETG showed finer and more uniform layering, reflecting their higher dimensional accuracy and rigidity. Micro-drilled specimens that are shown in Figure 9 demonstrated more complex morphologies near the hole and surrounding regions. The structural rearrangements and densification were observed in the vicinity of the drilled surface and were caused by the heat generation and fast cooling during the drilling process [14, 15, 18]. These thermal–mechanical effects likely altered the polymer microstructure, producing zones of differing morphology around the hole. Such microstructural heterogeneity can strongly influence mechanical behavior: modified layer alignment may hinder crack propagation in some cases, while increased defect density can exacerbate stress concentration and accelerate fracture in others. As presented in Table 4, tensile strength increased after micro-drilling in Tough PLA and PETG but decreased in ASA and Hyper PLA.

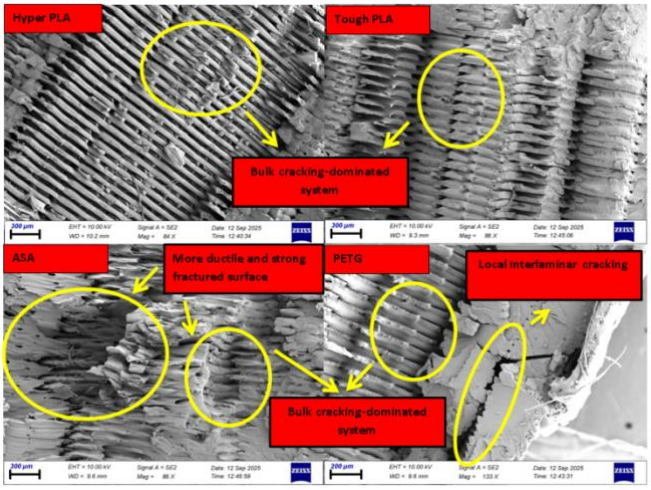

Figure 9. SEM micrographs of the fracture surfaces of the no-hole specimens after tensile testing.

Correspondingly, the SEM images show that ASA and Hyper PLA developed narrower, more irregular layers with numerous voids and interlayer discontinuities, whereas Tough PLA and PETG exhibited broader, more continuous lamellae. In particular, Tough PLA displayed excellent interfacial continuity between the drilled surface and adjacent layers, suggesting efficient stress transfer and contributing to its superior performance. The drilled surfaces of Tough PLA and PETG also appeared smoother than those of ASA and Hyper PLA.

Printed-hole specimens exhibited fracture surfaces taken from regions just beyond the hole perimeter, where ring-like fractures were previously noted. These regions lacked the ordered layered morphology seen in the no-hole and micro-drilled counterparts. These are shown in Figure 11. Among the four polymers, PETG showed the most irregular and brittle fracture surface, whereas ASA appeared least affected by the printed-hole geometry, maintaining relatively cohesive interlayer adhesion.

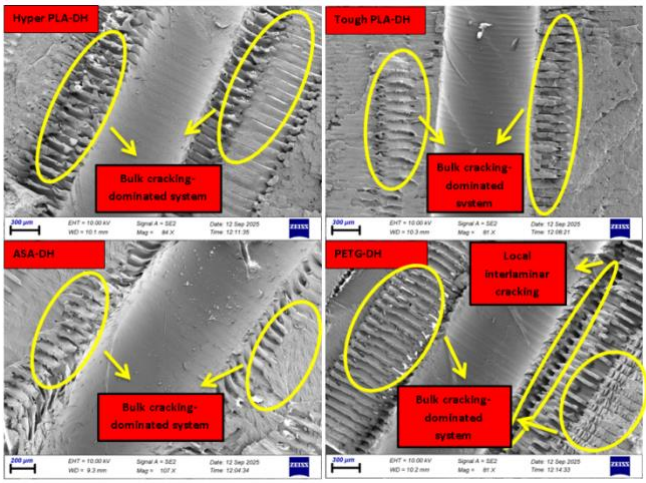

Figure 10. SEM micrographs of the fracture surfaces of the drilled-hole specimens after tensile testin.

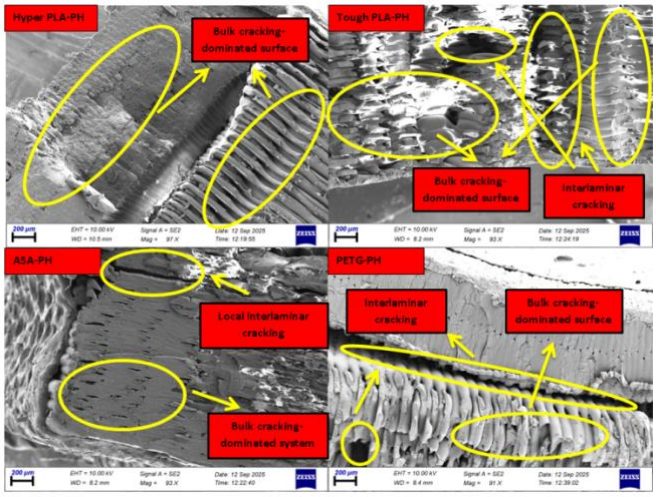

Figure 11. SEM micrographs of the fracture surfaces of the printed-hole specimens after tensile testing.

The observed fracture morphologies can be correlated with each material's softening temperature and melt flow index (MFI), as summarized for the four 3D-printed polymers in Table 5. Materials with higher MFI and lower softening points such as ASA tended to exhibit more ductile fracture and better accommodation of localized stress, while stiffer materials with lower flowability such as PETG were more susceptible to interlayer decohesion and brittle fracture around geometrical discontinuities.

Table 5. The softening temperature and MFI values of the produced four different materials (no-hole specimens).

Samples	Softening Temperature (°C)	Melting Flow Index (MFI, g/10min)	MFI of commercial filaments (MFI, g/10min)
ASA	108	16.5 (5kg)	22 (10 kg)
Tough PLA	69-67	9.7	17.3
Hyper PLA	67-65	14.7	17.3
PETG	80	24.0	20

Following FDM fabrication, tensile strength increased in the drilled-hole (DH) specimens of Tough PLA and PETG, whereas a reduction was observed for ASA and Hyper PLA compared with their respective no-hole counterparts. These opposite trends can be explained by analyzing the thermal and rheological properties of each polymer, especially their Vicat softening temperatures and melt flow indices (MFI) [13,20]. Among the tested materials, ASA exhibited the highest softening temperature (108 °C), suggesting that it is the least susceptible to localized heat accumulation during drilling. Consequently, while the stiffness (Young's modulus) of ASA-DH increased due to densification and strain hardening near the drilled region, the overall tensile strength decreased. This reduction can be attributed to enhanced stress concentrations and brittle crack initiation along the rougher drilled surface, as evidenced by SEM images showing narrower layer bands and irregular microstructural patterns near the hole edges. In contrast, polymers with lower softening temperatures such as Tough PLA, Hyper PLA, and PETG displayed

more uniform and wider interlayer bands around the drilled regions, indicating improved thermal accommodation and interfacial adhesion between the hole surface and adjacent layers. However, the fracture morphology of Hyper PLA-DH revealed pronounced distortions and irregular protrusions at the hole periphery, implying local structural degradation. This behavior may be associated with the thermal instability of certain plasticizing or flow-modifying additives within the Hyper PLA formulation [23,24]. Given that Hyper PLA is engineered for high-speed printing and high melt flow [25], its plasticizers may have partially degraded during localized heating in the drilling stage, leading to interlayer discontinuities and reduced mechanical strength.

Upon analyzing the fracture behavior of the specimens, it is found that the extent of the predominant failure mechanism is highly sensitive to the hole-making process. SEM analysis suggests that the printed-hole (PH) specimens failed mainly due to interlayer cracking and delamination. In these specimens, the ring-shaped fracture zones and irregular interlayer discontinuities around the hole boundary clearly indicate that the poor interlayer bonding is responsible for the crack propagation. On the other hand, although localized interlayer cracking was noticed occasionally in both drilled-hole (DH) and no-hole (NH) specimens, the overall fracture mechanism in these specimens was found to be governed mainly by bulk-dominated cracking processes. In DH specimens, the crack initiation sites were found to be mainly at the boundary of the drilled hole due to stress concentration, and the interlayer continuity was found to be largely unaffected. In a similar manner, the fracture surfaces of NH specimens were found to be mainly dominated by bulk deformation and crack propagation along the deposited filaments, rather than interlayer interfaces. These results are found to be in excellent agreement with the mechanical test results, where the PH specimens showed a significant reduction in tensile strength and ductility, whereas the DH and NH specimens showed a relatively higher load-carrying capacity. In general, although interlayer defects locally affect the fracture process in all FDM-printed specimens, the interlayer-dominated failure process is mainly accentuated in PH specimens, whereas the bulk-dominated cracking process is found to dominate the fracture behavior of DH and NH specimens.

The mechanical properties are also found to be affected by the hole-edge surface roughness, and these values are found to be in excellent agreement with the SEM images. The values of surface roughness are given in Table 4.

The measured values of hole edge roughness (Ra) provide a direct quantitative explanation for the differences in mechanical properties between printed-hole (PH) and drilled-hole (DH) specimens. As indicated in Table 4, the DH specimens had significantly lower Ra values than PH specimens for all tested materials, which directly confirmed the improved surface integrity of drilled holes. The lower surface roughness resulted in smoother hole edges, thus reducing stress concentrations and delaying the crack initiation process during tensile testing. Consequently, the DH specimens exhibited higher tensile strength and, more importantly, higher elongation at break than PH specimens.

Conversely, the PH specimens exhibited significantly higher Ra values due to layer stair-stepping, filament overlap, and incomplete interlayer bonding, which are common features of FDM-printed specimens. These surface features act as micro-notches that facilitate early crack initiation at the hole edge and cause premature failure. The influence of surface roughness was more pronounced for PETG and Tough PLA specimens, in which the higher Ra value was accompanied by a significant reduction in elongation at break, which clearly indicated a high sensitivity of ductility to hole-edge surface quality.

The inverse relationship between surface roughness (Ra) and mechanical properties has been extensively documented in the literature. Lower Ra values are known to be associated with higher tensile strength and improved ductility, whereas increased surface roughness results in the development of stress concentrators that facilitate early crack initiation and subsequent premature failure during tensile testing [10,26,27].

In the current research, the specimens were printed with a layer thickness of 50 μm, which is a setup that promotes the accumulation of heat and the overlap of loads. The thin layer setup could have also contributed to the effects of heat and stress during the drilling process. When the mechanical data of commercial filaments (Table 1) are compared with the properties of the 3D-printed specimens (Table 4), Hyper PLA shows the highest tensile strength and modulus both before and after printing; however, its relative improvement after printing is smaller than that of Tough PLA. The most prominent result, however, is the marked decrease in elongation at break measured for Tough PLA after printing. This strong decrease in elongation at break, together with the strong decrease in MFI (from 17.3 g/10 min in the filament to 9.7 g/10 min after printing), indicates an increase in molecular branching or cross-linking during the thermal processing step. It is hypothesized that Tough PLA contains reactive modifiers or chain extenders such as elastomeric tougheners or epoxy/anhydride-based additives (e.g., Joncryl ADR-type additives) that could potentially participate in secondary reactions during the multiple heating cycles of FDM printing. These reactions are expected to have increased the molecular weight and the density of chain entanglements, thus reducing the melt flowability and elongation at break, while slightly increasing the modulus and strength [28–30]. On the other hand, Hyper PLA, being formulated for high flow rates and rapid printing, is probably formulated with stable plasticizers and nucleating agents that can suppress chain reactions during post-processing. Consequently, the MFI of Hyper PLA would have decreased moderately (from 17.3 to 14.7 g/10 min), with less severe reduction in elongation. The differences in rheological properties between Tough PLA and Hyper PLA would thus account for their different mechanical behaviors after drilling. Finally, the increase in tensile strength of PETG-DH can be attributed to its highly amorphous structure [13,20]. Localized heating during drilling may have induced some crystallization or densification, thus increasing the load transfer and tensile strength. With PETG's moderate softening temperature (≈ 80 °C), such partial structural changes may have occurred without significant thermal degradation, thus positively contributing to its performance, since its softening point is not as high as ASA.

It is worth noting that all the open-hole specimens in the current study were produced under the same micro-hole diameter to provide a similar geometric stress concentration environment. Therefore, the differences in the mechanical behavior and failure process were primarily ascribed to the hole creation method and the local microstructural integrity around the holes rather than the hole size. The study of the effect of hole diameter on the stress concentration, such as stress concentration factors or numerical stress analysis, is believed to be a beneficial extension of the current study for future studies.

4. Conclusion

The key results of this research are presented below:

• The hole-making process affects the mechanical properties of FDM-printed polymers significantly.

• In-situ printed holes (PH) always demonstrated the lowest tensile strength, Young's modulus, and elongation at break values due to size inaccuracies and interlayer gaps.

• Micro-drilled holes (DH) always enhanced the stiffness of all materials, with up to 15% higher Young's modulus values.

• Tensile strength increased after drilling in PETG and Tough PLA, but decreased in ASA and Hyper PLA compared to the no-hole samples.

• SEM analysis confirmed that micro-drilled holes always produced more dense and smooth areas around the hole, while printed holes produced ring-shaped failure areas and poor interlayer bonding.

• The mechanical properties of the materials were strongly dependent on their Vicat softening temperatures and melt flow indices.

• Materials with moderate softening temperatures and balanced flow properties (PETG and Tough PLA) were more adaptable to the drilling process.

• High-Tg materials (ASA) and additive-modified materials (Hyper PLA) were more susceptible to localized thermal and mechanical phenomena during drilling.

• From a practical point of view, micro-drilling can be regarded as a robust post-processing technique to maintain or improve the mechanical properties of selected FDM materials, while in-situ printed holes should not be used in applications where high reliability is required.

Ethics committee approval and conflict of interest statement

This article does not require ethics committee approval and has no conflicts of interest with any individual or institution.

Acknowledgment

The authors declare that this study received no specific financial support from any funding agency in the public, commercial, or not-for-profit sectors.

Author Contribution Statement

The authors jointly contributed to the conceptualization, data analysis, interpretation of the results, and writing of the manuscript.

Declaration of Generative AI

During the preparation of this study, generative artificial intelligence tools were used solely for language and writing editing. All scientific content was developed by the authors.

References

[1] Li X, Tabil LG, Panigrahi S. Chemical treatments of natural fiber for use in natural fiber-reinforced composites: A review. J Polym Environ 2007;15:25-33. doi:10.1007/s10924-006-0042-3.

[2] Rajan K, Samykano M, Kadirgama K, Harun WSW, Rahman MM. Fused deposition modeling: Process, materials, parameters, properties and applications. Int J Adv Manuf Technol 2022;120:1531-1570. doi:10.1007/s00170-021-07860-5.

[3] Gibson I, Rosen D, Stucker B, Khorasani M. Additive manufacturing technologies. 2nd ed. Cham: Springer; 2021, p. 160-186. doi:10.1007/978-3-030-56127-7.

[4] Venkatesan K, Devendiran S, Bhupatiraju SCSR, Kolluru S, Kumar CP. Experimental investigation and optimization of micro-drilling parameters on Inconel 800 superalloy. Mater Manuf Process 2020;35:1214-1227. doi:10.1080/10426914.2020.1746812.

[5] Sen M, Eryilmaz O, Bakir B. Micro drilling characterization of the carbon and carbon-aramid (hybrid) composites. Polym Compos 2024;45:5449-5459. doi:10.1002/pc.28138.

[6] Schmeier GEC, Tröger C, Kwon YW, Sachau D. Predicting failure of additively manufactured specimens with holes. Materials 2023;16:2293. doi:10.3390/ma16062293.

[7] Sapora A, Torabi AR, Etesam S, Cornetti P. Finite fracture mechanics crack initiation from a circular hole. Fatigue Fract Eng Mater Struct 2018;41:1627-1636. doi:10.1111/ffe.12801.

[8] Iyibilgin O. Investigation of the effect of layer thickness on the mechanical properties of 316L austenitic stainless steel in additive manufacturing with metal filament. Appl Sci 2025;15:2584. doi:10.3390/app15052584.

[9] Ahmad MN, Yahya A. Effects of 3D printing parameters on mechanical properties of ABS samples. Designs 2023;7:136. doi:10.3390/designs7060136.

[10] Rankouhi S, Javadpour S, Delfanian F, Letcher T. Failure analysis and mechanical characterization of 3D printed ABS with respect to layer thickness and orientation. J Fail Anal Prev 2016;16:467-481. doi:10.1007/s11668-016-0117-0.

[11] Hernandez D. Factors affecting dimensional precision of consumer 3D printing. Int J Aviat Aeronaut Aerosp 2015;2(4). doi:10.15394/ijaaa.2015.1085.

[12] Knoop F, Schöppner V. Geometrical accuracy of holes and cylinders manufactured with fused deposition modeling. In: 28th Annual International Solid Freeform Fabrication Symposium; 2017. p. 2757–2776.

[13] Ramian J, Dziob D. Thermal deformations of thermoplast during 3D printing: Warping in the case of ABS. Materials 2021;14:7070. doi:10.3390/ma14227070.

[14] Lv W, Qin X, Bao Z, Guo W, Meng X, Li H. Comparison of joining hole-making methods for fiber-reinforced FDM 3D printing parts. Proc Inst Mech Eng Part B J Eng Manuf 2024;238:2075-2091. doi:10.1177/09544054231223265.

[15] Gómez-Gras G, Pérez MA, Fábregas-Moreno J, Reyes-Pozo G. Experimental study on the accuracy and surface quality of printed versus machined holes in PEI Ultem 9085 FDM specimens. Rapid Prototyp J 2021;27:1-12. doi:10.1108/RPJ-12-2019-0306.

[16] Rao S, Paul R, Singh S, Debnath K. Influence of conventionally drilled and additively fabricated holes on tensile properties of 3D-printed ONYX/CGF composites. J Mater Eng Perform 2023;32:5849-5861. doi:10.1007/s11665-022-07529-2.

[17] Sen M, Eryilmaz O, Bakir B. Multi-objective process optimization of micro-drilling parameters on carbon and carbon-aramid (hybrid) fabric composites. Arab J Sci Eng 2025;50:9535-9552. doi:10.1007/s13369-024-09616-z.

[18] Dizon RC, Gache CCL, Cascolan HMS, Cancino LT, Advincula RC. Post-processing of 3D-printed polymers. Technologies 2021;9:61. doi:10.3390/technologies9030061.

[19] All3DP. 3D printing materials guide. 2025. Available from: https://all3dp.com/1/3d-printing-materials-guide-3d-printer-material/ [Accessed 1 August 2025].

[20] Dey I, Roan Eagle N, Yodo N. A review on filament materials for fused filament fabrication. J Manuf Mater Process 2021;5:69. doi:10.3390/jmmp5030069.

[21] Porima 3D. 3D printer filaments. 2025. Available from: https://porima3d.com [Accessed 5 August 2025].

[22] ASTM International. ASTM D638-10: Standard test method for tensile properties of plastics. 2010. doi:10.1520/D0638-10.

[23] Mastalygina EE, Aleksanyan KV. Recent approaches to the plasticization of poly(lactic acid) (PLA): A review. Polymers 2023;16:87. doi:10.3390/polym16010087.

[24] Brdlík P, Novák J, Borůvka M, Běhálek L, Lenfeld P. The influence of plasticizers and accelerated ageing on biodegradation of PLA under controlled composting conditions. Polymers 2023;15:140. doi:10.3390/polym15010140.

[25] Porima. Porima Hyper PLA filament: Product description. 2025. Available from: https://www.filamenthane.com/urun/porima-hyper-pla-filament [Accessed 10 October 2025].

[26] Kuruoglu Y, Akgun M, Demir H. Modeling and optimization of surface roughness and tensile strength of ABS, PLA, and PETG specimens produced by the FDM method. Int J 3D Print Technol Digit Ind 2022;6:358-369. doi:10.46519/ij3dptdi.1148923.

[27] Dizon JRC, Espera AH Jr, Chen Q, Advincula RC. Mechanical characterization of 3D-printed polymers. Addit Manuf 2018;20:44-67. doi:10.1016/j.addma.2017.12.002.

[28] Srisuwan Y, Baimark Y, Suttiruengwong S. Toughening of poly(L-lactide) with blends of poly(ε-caprolactone-co-L-lactide) in the presence of chain extender. Int J Biomater 2018;2018:1294397. doi:10.1155/2018/1294397.
[29] Rasselet D, Caro-Bretelle AS, Taguet A, Lopez-Cuesta JM. Reactive compatibilization of PLA/PA11 blends and their application in additive manufacturing. Materials 2019;12:485. doi:10.3390/ma12030485.
[30] Grigora M-E, Terzopoulou Z, Tsongas K, Klonos P, Kalafatakis N, Bikiaris DN, et al. Influence of reactive chain extension on the properties of 3D-printed poly(lactic acid) constructs. Polymers 2021;13:1381. doi:10.3390/polym13091381.